

---

# Size Generalizability of Graph Neural Networks on Biological Data: Insights and Practices from the Spectral Perspective

---

**Yujun Yan\***

Dartmouth College  
yujun.yan@dartmouth.edu

**Gaotang Li\***

University of Michigan, Ann Arbor  
gaotang@umich.edu

**Danai Koutra**

University of Michigan, Ann Arbor  
dkoutra@umich.edu

## Abstract

We investigate the question of whether the knowledge learned by graph neural networks (GNNs) from small graphs is generalizable to large graphs in the same domain. Prior works suggest that the distribution shift, particularly in the degree distribution, between graphs of different sizes can lead to performance degradation in the graph classification task. However, this may not be the case for biological datasets where the degrees are bounded and the distribution shift of degrees is small. Even with little degree distribution shift, our observations show that GNNs' performance on larger graphs from the same datasets still degrades, suggesting other causes. In fact, there has been a lack of exploration in real datasets to understand the types and properties of distribution shifts caused by various graph sizes. Furthermore, previous analyses of size generalizability mostly focus on the spatial domain. To fill these gaps, we take the spectral perspective and study the size generalizability of GNNs on biological data. We identify a distribution shift between small and large graphs in the eigenvalues of the normalized Laplacian/adjacency matrix, indicating a difference in the global node connectivity, which is found to be correlated with the node closeness centrality. We further find that despite of the variations in global connectivity, graphs of different sizes share similar local connectivity, which can be utilized to improve the size generalizability of GNNs. Based on our spectral insights and empirical observations, we propose a model-agnostic strategy, SIA, which uses size-irrelevant local structural features, i.e., the local closeness centrality of a node, to guide the learning process. Our empirical results demonstrate that our strategy improves the graph classification performance of various GNNs on small and large graphs when training with only small graphs.

## 1 Introduction

We focus on the size generalizability of graph neural networks on biological data. While numerous GNNs [17, 27, 13, 38, 34, 19] have exhibited exceptional performance in graph classification tasks and can handle graphs of varying size, there has been inadequate research into the ability of GNNs to generalize effectively from small to large graphs. Size generalizability is a critical concern in various fields. For instance, in graph algorithmic reasoning, neural networks (NN) learn complex

---

\*Equal Contribution.

algorithms from small graph examples and generalize that reasoning to larger graphs, as obtaining exact solutions for larger graphs is challenging. In the biological domain, datasets can vary in graph size, from small atom-based structures to large compounds with thousands of atoms. It is important to assess if the learned knowledge is influenced by graph size, as size-dependent information could adversely affect performance when using pre-training strategies [15].

Many prior works [36, 7, 5] have observed performance degradation when there exists a size shift between the training and test data. However, it remains unclear: what structural properties will change with the graph size? The answer to this question depends on the data domain. For instance, local degree patterns in social networks may vary with graph size [36] while the node degrees in biological networks are bounded and the difference in degree distributions between small and large graphs is small (Section 5.2). Additionally, the global connectivity of nodes in biological graphs may change with the graph size. Many prior works [7, 5, 35], however, lack sufficient exploration and verification on real datasets to understand the types and properties of distribution shifts caused by various graph sizes. Thus, it is unclear what distribution shifts they target at and what data domain their methods can improve the size generalizability on. In this paper, we obtain two important observations from biological data: (1) the eigenvalue distributions, obtained from the normalized Laplacian/adjacency matrix, vary with the graph size. The differences in the eigenvalue distributions reflect the variations in the global connectivity of the nodes, which are associated with the node closeness centrality; and (2) graphs with different sizes have similar distributions of local node connectivity, which can be measured by the local closeness centrality computed from the subgraphs induced from local neighborhoods. We use these observations to guide our design of a Size-Insensitive Attention (SIA) strategy, which is model agnostic and helps improve the size generalizability of many GNN models.

Furthermore, most analyses in prior works [36, 7, 5] focus on the spatial domain. In this paper, we take the spectral perspective to understand why GNNs can be sensitive to size shift, and use the insights from the spectral domain to understand what structural properties change with the graph size. In sum, our paper makes the following contributions:

- **New Observations.** We identify the types and properties of distribution shifts caused by various graph sizes in biological networks.
- **Spectral Analyses.** Unlike prior works in size generalizability, we take the spectral perspective and use the spectral insights to analyze the structural change with the graph size.
- **Model Agnostic Strategy.** Based on our spectral insights and empirical observations, we propose a model agnostic strategy, SIA, which uses size-irrelevant local structural features, i.e., the local closeness centrality of a node, to guide the learning process.

## 2 Notations and Preliminaries

In this section, we introduce the definitions and notations that are used throughout the paper. Let  $\mathcal{G}(\mathcal{V}, \mathcal{E})$  be an undirected and unweighted graph with  $N$  nodes, where  $\mathcal{V}$  denotes the node set, and  $\mathcal{E}$  denotes the edge set. The  $h$ -hop neighborhood of a node  $v_i$  is defined as the set of all nodes that are at a distance of  $h$  or less from the node  $v_i$ :  $\mathcal{N}_i^h = \{v_j | \text{dist}(v_j, v_i) \leq h\}$ . We use  $\mathbf{A}$  to represent the adjacency matrix of the graph,  $\mathbf{D}$  to represent the degree matrix whose  $i$ th diagonal element is the degree of node  $v_i$ .

### 2.1 Closeness Centrality

**Global Closeness Centrality.** Global closeness centrality [3] of a node  $v_i$  measures how long it will take information to spread from  $v_i$  to other nodes in the network. It is calculated as the reciprocal of the average length of the shortest paths between  $v_i$  and all other nodes in the graph. To account for graphs with more than one connected component, we adopt the following closeness definition in [26]:

$$C(v_i) = \frac{n-1}{N-1} \frac{n-1}{\sum_{j=1}^{n-1} \text{dist}(v_i, v_j)},$$

where  $n$  is the number of reachable nodes from  $v_i$ .

**$h$ -hop Closeness Centrality.**  $h$ -hop closeness centrality is a variant of closeness centrality proposed in this paper, which aims to capture the local connectivity of the nodes. It is computed using the

subgraphs induced from  $h$ -hop neighborhood of the node  $v_i$ :

$$C^{(h)}(v_i) = \frac{|\mathcal{N}_i^h| - 1}{\sum_{v_j \in \mathcal{N}_i^h, v_j \neq v_i} \text{dist}(v_i, v_j)}$$

## 2.2 Graph Learning Task

In this paper, we focus on the graph classification task, where each node  $v_i$  is associated with a feature vector  $\mathbf{x}_i^{(0)}$ , and the feature matrix  $\mathbf{X}^{(0)}$  is constructed by arranging the node feature vectors as rows. When using a GNN for the graph classification task, we further denote the node representation matrix at the  $l$ -th layer as  $\mathbf{X}^{(l)}$ , and the representation of node  $v_i$  as  $\mathbf{x}_i^{(l)}$ .

**Supervised Graph Classification.** Each graph  $\mathcal{G}_i$  is associated with a ground truth label  $y_i^{\mathcal{G}}$  sampled from a label set  $\hat{\mathcal{L}}$ . Given a subset of labeled graphs (from a label set  $\hat{\mathcal{L}}$ ), the goal is to learn a mapping  $f^{\mathcal{G}} : (\mathbf{A}, \mathbf{X}^{(0)})_i \mapsto y_i^{\mathcal{G}}$  between each graph  $\mathcal{G}_i$  and its ground truth label  $y_i^{\mathcal{G}} \in \hat{\mathcal{L}}$ . The graph classification loss is given by  $L = \frac{1}{|\mathcal{G}_{\text{train}}|} \sum_{\mathcal{G}_i \in \mathcal{G}_{\text{train}}} \text{CrossEntropy}(\mathbf{x}^{\mathcal{G}_i}, y_i^{\mathcal{G}})$ , where  $\mathcal{G}_{\text{train}}$  is the training graph set and  $\mathbf{x}^{\mathcal{G}_i}$  is the representation of graph  $\mathcal{G}_i$ .

## 2.3 Graph Neural Networks for Graph Classification

GNNs can be designed from either the spatial perspective or the spectral perspective. Despite the difference in the design perspectives, a recent work [1] has shown that spectral GNNs and spatial GNNs are related and that spectral analysis of GNNs' behavior can provide a complementary point of view to understand GNNs in general.

**Spatial Perspective.** Many GNNs [17, 31, 27, 13] use the message passing framework [12], which is consisted of three steps: neighborhood propagation and aggregation, combination and global pooling. The node representations at  $l$ -th layer are given by:  $\mathbf{x}_i^{(l+1)} = \text{Combine}(\text{Aggregate}(\mathbf{x}_j^{(l)}, v_j \in \mathcal{N}_i^1, v_j \neq v_i), \mathbf{x}_i^{(l)})$ , where the function **Aggregate** can be **Sum** [31], **Average** [17], or other learned aggregating functions [27]; and the function **Combine** can be **Concat** [13] or **Average** [17]. The graph representation is obtained from the node representations at the last layer:  $\mathbf{x}^{\mathcal{G}} = \text{Pooling}(\{\mathbf{x}_i^{(\text{Last})}\})$ , where the **Pooling** function is performed on the set of all the node representations, and it can be **Global\_mean** or **Global\_max** or other more complex pooling functions [37, 18].

**Spectral Perspective.** Spectral GNNs [6, 11, 21] utilize the spectral properties of a propagation matrix  $\mathbf{T}$  to perform the graph classification. The propagation matrix  $\mathbf{T}$  is usually a function of the adjacency matrix  $\mathbf{A}$ , such as the normalized adjacency matrix  $\mathbf{T} = (\mathbf{D} + \mathbf{I})^{-1/2}(\mathbf{A} + \mathbf{I})(\mathbf{D} + \mathbf{I})^{-1/2}$ , or the normalized graph Laplacian matrix  $\mathbf{T} = \mathbf{I} - \mathbf{D}^{-1/2}\mathbf{A}\mathbf{D}^{-1/2}$ . We consider an undirected graph with a real and symmetric adjacency matrix. Consequently, the propagation matrix  $\mathbf{T}$  is also real and symmetric. Then we can perform the eigendecomposition on the propagation matrix  $\mathbf{T}$ :  $\mathbf{T} = \mathbf{U}\mathbf{\Lambda}\mathbf{U}^T$ , where  $\mathbf{U}$  is an orthogonal matrix whose columns  $\mathbf{U}_i$  are orthonormal and are the eigenvectors of  $\mathbf{T}$ ;  $\mathbf{\Lambda}$  is a matrix whose diagonal elements are the eigenvalues of  $\mathbf{T}$ , sorted from large to small by their absolute values. The set of eigenvectors  $\{\mathbf{U}_i\}$  form the orthonormal basis of  $\mathbb{R}^n$ . The goal of a spectral GNN is to learn a proper spectral filter:  $f(\mathbf{\Lambda}) = c_0\mathbf{I} + c_1\mathbf{\Lambda} + c_2\mathbf{\Lambda}^2 + \dots + c_i\mathbf{\Lambda}^i + \dots$ , where  $c_i$  are the learnable coefficients. The convolution at each layer can be viewed as or is equivalent to:  $\mathbf{X}^{(l+1)} = \sigma(\mathbf{U}f(\mathbf{\Lambda})\mathbf{U}^T\mathbf{X}^{(l)}\mathbf{W}^{(l)})$ , where  $\mathbf{W}^{(l)}$  is a learnable weight matrix, and  $\sigma(\cdot)$  is a nonlinear function (e.g., ReLU). Similar to the spatial GNNs, a global pooling is performed after the last convolution layer to obtain a graph representation for the graph classification task.

## 3 Size Generalizability from the Spectral Perspective

In this section, we take a spectral perspective to analyze the factors that affect the size generalizability of a GNN. At a high level, we study how the graph representation correlates with the graph size.

The output of a GNN at the  $(l+1)$ -th layer is given by:  $\mathbf{X}^{(l+1)} = \sigma(\mathbf{U}f(\mathbf{\Lambda})\mathbf{U}^T\mathbf{X}^{(l)}\mathbf{W}^{(l)})$  (Section 2). To ease our analysis, we rewrite  $\mathbf{U}$ ,  $\mathbf{\Lambda}$  and  $\mathbf{X}^{(l)}$  as:  $\mathbf{U} = [\mathbf{U}_1, \mathbf{U}_2, \dots, \mathbf{U}_N]$ ,  $\mathbf{\Lambda} = \text{Diag}([\lambda_1, \lambda_2, \dots, \lambda_N])$ , and  $\mathbf{X}^{(l)} = [\mathbf{X}_1^{(l)}, \mathbf{X}_2^{(l)}, \dots, \mathbf{X}_D^{(l)}]$ , respectively.  $\mathbf{U}_i$  is the  $i$ -th column

vector of  $\mathbf{U}$ ,  $\lambda_i$  is the  $i$ -th largest eigenvalue,  $\text{Diag}(\cdot)$  creates a matrix with the vector as its diagonal elements,  $\mathbf{X}_i^{(l)}$  is the  $i$ -th column vector of  $\mathbf{X}^{(l)}$ , and  $D$  is the feature dimension at the  $l$ -th layer.

$$\begin{aligned}\mathbf{X}^{(l+1)} &= \sigma([\mathbf{U}_1, \mathbf{U}_2, \dots, \mathbf{U}_N] \cdot \text{Diag}([f(\lambda_1), f(\lambda_2), \dots, f(\lambda_N)]) \cdot ([\mathbf{U}_1, \mathbf{U}_2, \dots, \mathbf{U}_N])^T \\ &\quad \cdot [\mathbf{X}_1^{(l)}, \mathbf{X}_2^{(l)}, \dots, \mathbf{X}_D^{(l)}] \cdot \mathbf{W}^{(l)}) \\ &= \sigma([f(\lambda_1)\mathbf{U}_1, f(\lambda_2)\mathbf{U}_2, \dots, f(\lambda_N)\mathbf{U}_N] \cdot ([\mathbf{U}_1, \mathbf{U}_2, \dots, \mathbf{U}_N])^T \\ &\quad \cdot [\mathbf{X}_1^{(l)}, \mathbf{X}_2^{(l)}, \dots, \mathbf{X}_D^{(l)}] \cdot \mathbf{W}^{(l)}).\end{aligned}\tag{1}$$

Since  $\{\mathbf{U}_i : i = 1, \dots, N\}$  are the orthonormal basis of  $\mathbb{R}^N$ ,  $\mathbf{X}_i^{(l)}$  can be expressed as a linear combination of  $\{\mathbf{U}_i\}$ . Thus, suppose  $\mathbf{X}_i^{(l)} = \sum_{j=1,2,\dots,N} \alpha_j^i \mathbf{U}_j$ , then Equation 1 can be rewritten as:

$$\begin{aligned}\mathbf{X}^{(l+1)} &= \sigma([f(\lambda_1)\mathbf{U}_1, f(\lambda_2)\mathbf{U}_2, \dots, f(\lambda_N)\mathbf{U}_N] \cdot ([\mathbf{U}_1, \mathbf{U}_2, \dots, \mathbf{U}_N])^T \\ &\quad \cdot [\sum_{j=1,2,\dots,N} \alpha_j^1 \mathbf{U}_j, \dots, \sum_{j=1,2,\dots,N} \alpha_j^D \mathbf{U}_j] \cdot \mathbf{W}^{(l)}) \\ &= \sigma \left( [f(\lambda_1)\mathbf{U}_1, f(\lambda_2)\mathbf{U}_2, \dots, f(\lambda_N)\mathbf{U}_N] \cdot \begin{bmatrix} \alpha_1^1 & \alpha_1^2 & \dots & \alpha_1^D \\ \alpha_2^1 & \alpha_2^2 & \dots & \alpha_2^D \\ \dots & \dots & \dots & \dots \\ \alpha_N^1 & \alpha_N^2 & \dots & \alpha_N^D \end{bmatrix} \cdot \mathbf{W}^{(l)} \right) \\ &= \sigma([\sum_{j=1,\dots,N} f(\lambda_j) \alpha_j^1 \mathbf{U}_j, \sum_{j=1,\dots,N} f(\lambda_j) \alpha_j^2 \mathbf{U}_j, \dots, \sum_{j=1,\dots,N} f(\lambda_j) \alpha_j^D \mathbf{U}_j] \cdot \mathbf{W}^{(l)}).\end{aligned}\tag{2}$$

We know that  $\alpha_j^i = \mathbf{U}_j^T \cdot \mathbf{X}_i^{(l)} = \text{COSINE}(\mathbf{U}_j, \mathbf{X}_i^{(l)}) \cdot \|\mathbf{X}_i^{(l)}\|_2 = \text{COSINE}(\mathbf{U}_j, \mathbf{X}_i^{(l)}) \cdot \frac{\|\mathbf{X}_i^{(l)}\|_2}{\sqrt{N}} \cdot \sqrt{N}$ . Then Equation 2 can be rewritten as:

$$\begin{aligned}\mathbf{X}^{(l+1)} &= \sigma([\sum_{j=1,\dots,N} f(\lambda_j) \text{COSINE}(\mathbf{U}_j, \mathbf{X}_1^{(l)}) \cdot \frac{\|\mathbf{X}_1^{(l)}\|_2}{\sqrt{N}} \cdot (\sqrt{N} \cdot \mathbf{U}_j), \\ &\quad \dots, \sum_{j=1,\dots,N} f(\lambda_j) \text{COSINE}(\mathbf{U}_j, \mathbf{X}_D^{(l)}) \cdot \frac{\|\mathbf{X}_D^{(l)}\|_2}{\sqrt{N}} \cdot (\sqrt{N} \cdot \mathbf{U}_j)] \cdot \mathbf{W}^{(l)}).\end{aligned}\tag{3}$$

The final graph representation is obtained through a global pooling (Section 2), where a set function is applied to each feature dimension. To ensure that the graph representation is irrelevant to the graph size, it is crucial for each column of  $\mathbf{X}^{(l+1)}$  to be unaffected by the size. If the distributions of eigenvalues ( $\lambda_j$ ) and scaled eigenvectors ( $\sqrt{N} \cdot \mathbf{U}_j$ ), as well as the scalar  $\frac{\|\mathbf{X}_i^{(l)}\|_2}{\sqrt{N}}$ , are uncorrelated with the graph size, then the graph representation will be size-invariant. It is worth noting that  $\mathbf{X}_i^{(l)}$  contains  $N$  elements and its 2-norm scales with  $\sqrt{N}$ ; and  $\|\mathbf{U}_j\|_2 = 1$  and its elements diminish with  $\sqrt{N}$ . Hence, we account for the scaling factor  $\sqrt{N}$  in both terms. However, as demonstrated in Section 5.2 and appendix D, the distributions of eigenvalues and scaled eigenvectors in real biological graphs are influenced by the graph size. This poses a challenge for the size generalization of GNNs. Importantly, the difference in eigenvalue distributions cannot be attributed to the value range [4], as the eigenvalues of a normalized Laplacian matrix and adjacency matrix are constrained within the intervals  $[0, 2]$  and  $[-1, 1]$  respectively.

## 4 Methodology

Before presenting our method, we highlight two observations discovered in biological networks, which will be thoroughly explained in Section 5. These observations serve as the motivation behind our development of a size-insensitive attention mechanism.

- **Observation 1:** The differences in the eigenvalue distributions reflect the variations in the global connectivity of the nodes, which are associated with the node closeness centrality.

- **Observation 2:** Graphs with different sizes have similar distributions of local node connectivity, which can be measured by the local closeness centrality computed from the subgraphs induced from local neighborhoods.

Motivated by Observation 2, our design aims at improving size generalizability by incorporating size-insensitive local structural features. Intuitively, we aim to utilize these structural features to filter out the nodes that increase in quantity with the graph size but are less relevant to the labels. Attention is a suitable mechanism in our setting as it can filter out irrelevant information [18] and be integrated with structural features. However, as noted in [28, 33], attention weights gradually lose fidelity with larger graphs. Therefore, our design focuses on two main challenges: (1) designing size-insensitive local structural features and (2) reducing the impact of graph size on the attention weights.

**Structural Feature Design.** Inspired by Observation 2, we use local closeness centrality as the node features. In more detail, we compute the local closeness centrality of a node  $v_i$  from its  $h$ -hop neighborhoods  $\mathcal{N}_i^h$ , where  $h$  is the largest neighborhood size to maintain size-insensitivity (Section 5.4). To enrich the features [10], we further compute the maximum, minimum, average, and standard deviation of  $h$ -hop closeness for the nodes in  $v_i$ ’s immediate neighborhood. In this way, for each node  $v_i$ , we manually construct a 5-dimensional feature vector  $\mathbf{c}_i$  such that

$$\mathbf{c}_i = [C^h(v_i), \max(\{C^h(v_j)\}), \min(\{C^h(v_j)\}), \text{avg}(\{C^h(v_j)\}), \text{std}(\{C^h(v_j)\})]^\top, v_j \in \mathcal{N}_i^1 \quad (4)$$

**Size-insensitive Structural Attention.** We use the structural feature matrix  $\mathbf{C} = [\mathbf{c}_1, \dots, \mathbf{c}_N]$ ,  $\mathbf{c}_i \in \mathbb{R}^5$  for attention. However, attention weights often diminish with increasing graph size due to the utilization of Softmax. To address this issue, we propose scaling the attention weights by the graph size and employing Global\_max as the global pooling operation to mitigate the impact of graph size. Mathematically, our final graph representation is given by:

$$\mathbf{k} = \text{Softmax}(\mathbf{w}_A^\top \mathbf{C}) \cdot N, \quad \mathbf{x}^G = \text{Global\_max}(\text{Diag}(\mathbf{k}) \cdot \mathbf{X}^{(\text{Last})}) \quad (5)$$

where  $\mathbf{w}_A^\top$  is a learnable vector, and  $\text{Diag}(\cdot)$  creates a diagonal matrix using the vector as its elements.

We perform a comprehensive ablation study on Appendix F to showcase the effectiveness of our feature selection. Our findings reveal that local closeness alone can enhance size generalizability to some extent. However, when incorporating more enriched features, the improvements become more consistent and pronounced.

## 5 Experiments

### 5.1 Overview of the Experimental Setup

In our experiments, we use three pre-processed biological datasets (BBBP, BACE, and PROTEINS) from the Open Graph Benchmark [16] and TuDataset [23] to perform graph classification. More details about the datasets are provided in Appendix A.

**Data Preprocessing and Important Training Details** In order to analyze size generalizability, we have four splits for each dataset: train, validation, small\_test, and large\_test, where large\_test contains graphs with significantly larger sizes. We generate the splits as follows. First, we sort the samples in the dataset by their size. Next, We take the train, validation, and small\_test split from the 50% smallest graphs in the dataset. An intuitive way of getting the large\_split is to take the top  $k$  largest graphs. However, doing so would result in severe label skewness (class imbalances) between the small\_test and the large\_test as demonstrated by Table 4 in Appendix B. To avoid such a severe distribution shift, we select the same number of graphs per class as in the small\_test subset, starting from the largest graph within each class. In this way, we ensure the label distribution between small\_test and large\_test is the same. Nevertheless, the smallest 50% samples still have significant **class imbalance**. To address this issue, we use upsampling during training throughout the experiments, and we use **F1** as the metric to measure the model performance. More details about data preprocessing, hyperparameters, and training can be found in Appendix B and Appendix C.

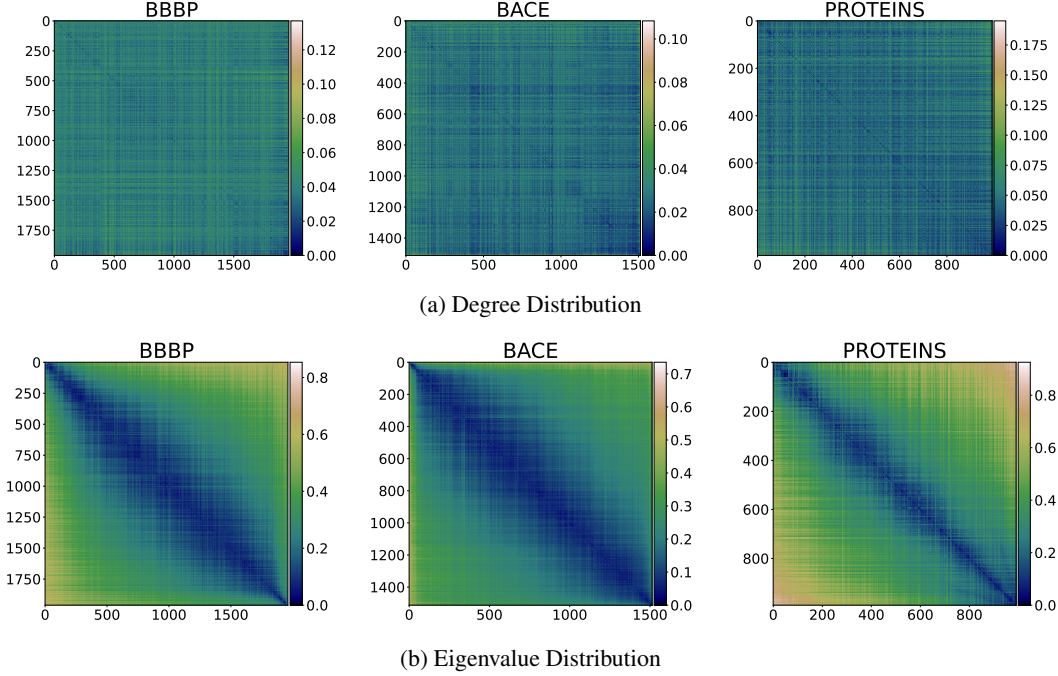


Figure 1: Graph distance is quantified using the Wasserstein distance for degree (a) and eigenvalue (b) distributions, respectively. Graphs are sorted from small to large, and the (i,j)-th pixel in the plot represents the distance between the i-th and j-th graphs. Dark blue represents a small distance (high similarity), while light red represents a large distance (low similarity). We find that **degree distributions do not show a clear correlation with the graph size** and **eigenvalue distributions show a strong correlation with the graph size**.

Table 1: Average Wasserstein distance between graphs of similar sizes and graphs of different sizes based on **degree** and **eigenvalue** distributions, respectively. The relative difference is computed by the difference of the Wasserstein distance normalized by the Wasserstein distance of similar graphs.

Datasets	Degree Distribution Difference			Eigenvalue Distribution Difference		
	Different sizes	Similar sizes	Relative difference	Different sizes	Similar sizes	Relative difference
BBBP	0.039	0.035	12.1%	0.281	0.091	209%
BACE	0.027	0.024	14.7%	0.204	0.073	177%
PROTEINS	0.047	0.041	14.8%	0.379	0.130	192%

## 5.2 Dependence of Structural Properties on Graph Size

In this subsection, we aim to address the question: “What structural properties change with the graph size?” To explore this, we focus on two structural properties of the graphs: degree distribution and eigenvalue distribution. We present their relationship with the graph size in Figure 1.

Figure 1 illustrates the pairwise distances of the graphs arranged in ascending order of size, where the distances are calculated using the Wasserstein distance [29]. We measure the empirical distributions of degrees (Figure 1a) and eigenvalues (Figure 1b), respectively, to compute these distances. The eigenvalues are obtained from the normalized adjacency matrix as suggested in [17]:  $\mathbf{T} = (\mathbf{D} + \mathbf{I})^{-1/2}(\mathbf{A} + \mathbf{I})(\mathbf{D} + \mathbf{I})^{-1/2}$ . We have similar observations for normalized Laplacian matrix. Note that the eigenvalues do not scale with the graph size, and they are bounded between  $[-1, 1]$ . Dark blue represents a small distance (high similarity) while light red represents a large distance (low similarity). We find that Figure 1a does not have a clear pattern and thus the graph distance measured by degree distributions does not show a clear correlation with the graph size. In contrast, there is a wide blue band along the diagonal in the three subplots in Figure 1b, corresponding to the three datasets in our analysis. This indicates that graphs of similar sizes have more similar eigenvalue distributions than graphs of different sizes. It suggests a strong correlation between the eigenvalue distributions and the graph size. To verify the analysis quantitatively, we compute the distance of graphs with similar sizes and graphs of different sizes in Table 1. Graphs of similar sizes include 20

graphs whose size is closest to the graph of interest, and graphs of different sizes are the remaining graphs. From the table, we find that (1) the Wasserstein distance of degree distributions between the graphs of different sizes are slightly larger (around 15%) than the distance between graphs of similar sizes; and (2) the Wasserstein distance of eigenvalue distributions between the graphs of different sizes are significantly larger than the distance between graphs of similar sizes. This implies that the discrepancy of degree distributions is not the main challenge to the size generalizability of GNNs on real biological graphs. Furthermore, based on the results and the analysis in Section 3, the correlation between the eigenvalue distributions and the graph size results in the correlation of the final graph representation and the graph size, which prevents GNNs from generalizing over different sizes.

### 5.3 Observation 1

In this subsection, we present our first observation that the discrepancies of the eigenvalue distributions reflect the differences of global connectivity of the nodes, which are correlated with the node closeness centrality. Our intuition is that the structural connectivity of the graph is often related to the eigenvalues of the normalized Laplacian matrix. For example, the algebraic multiplicity of eigenvalue 0 represents the number of connected components in the graph [9]; the cheeger constant [8], which measures the "bottle neck" of the graph, is related to the spectral gap of the graph. To analyze their relationship, we compute the empirical distribution of node closeness centrality for each graph (Section 2) as an indicator of global node connectivity and examine its correlation with the eigenvalue distribution. To elaborate, we randomly select 200 pairs of graphs. Each pair of graphs yields two distances: one calculated from the eigenvalue distributions and the other from the closeness distributions. We then map each graph pair to a point whose coordinates represent the two distances. The scatter plots for three datasets are depicted in Figure 2. The  $x$ -axis represents the closeness distance, and the  $y$ -axis represents the eigenvalue distance. We find that there is a clear correlation between the two variables in all the plots we draw. To verify it quantitatively, we compute the Pearson correlation between the two distances, and the result is presented in Figure 2. To conclude, the closeness distribution is highly or moderately correlated with the eigenvalue distributions in real-world biological datasets.

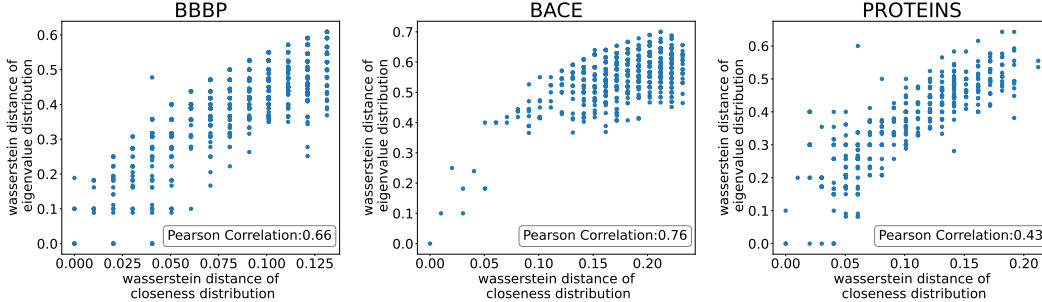


Figure 2: Correlation between the distances measured by eigenvalue distributions and closeness distributions on BBBP, BACE, and PROTEINS datasets. The closeness distribution is highly or moderately correlated with the eigenvalue distribution.

### 5.4 Observation 2

In this subsection, we present our second observation that graphs with different sizes have similar distributions of local node connectivity. We measure the local node connectivity by computing the closeness of a node in its local neighborhoods. In the following analysis, we use the BACE dataset as an example, and similar analyses are conducted for the other two datasets in Appendix E.

Following the same procedures in Section 5.2, Figure 3 shows the distances of sorted graphs, where the distance is measured by the Wasserstein distance between the empirical distributions of  $h$ -hop local closeness. We can see that in the two-hop and three-hop plots, small and large graphs share similar distributions of local closeness. In contrast, there is a clear wide blue band along the diagonal in the four-hop plot, indicating that the graph distance measured by four-hop local closeness correlates with the graph size. To verify the analysis quantitatively, we compute the distance of graphs of similar sizes and graphs of different sizes in Table 2. We follow the same definitions in Section 5.2. We

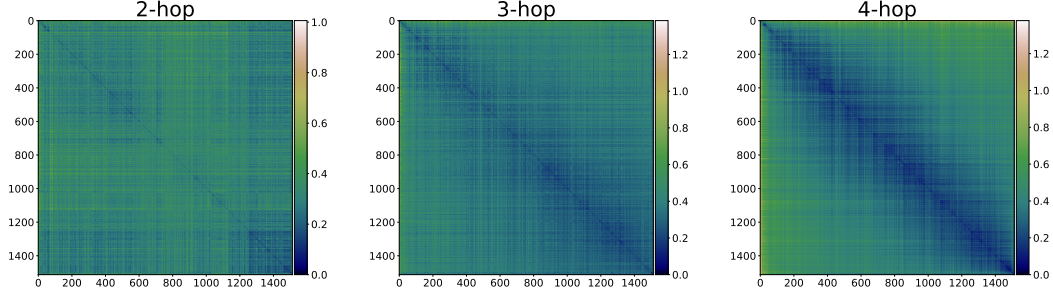


Figure 3: Graph distance based on  $h$ -hop local closeness for BACE (left to right:  $h=2$ ,  $h=3$ , and  $h=4$ ). Graphs are sorted from small to large and we follow the same procedures as Figure 2. Small-hop (two-hop and three-hop) local closeness does not exhibit a clear dependence on graph size.

Table 2: Average Wasserstein distance between graphs of similar sizes and graphs of different sizes based on  **$h$ -hop local closeness** for BACE. The relative difference is computed by the difference of the average Wasserstein distance normalized by the average Wasserstein distance of similar graphs.

Number of Hops	Different sizes	Similar sizes	Relative Difference
<b>2-hop</b>	0.314	0.268	17.1%
<b>3-hop</b>	0.368	0.265	38.5%
<b>4-hop</b>	0.387	0.201	92.2%

observe that the relative difference between graphs of similar sizes and graphs of different sizes are relatively small for two-hop and three-hop local closeness, but becomes significant for four-hop local closeness. This quantitative result verifies the plot shown in Figure 3. We thus conclude that three-hop is the maximum neighborhood size in the BACE dataset that preserves the size-insensitivity of the local closeness features. As a consequence, we choose  $h = 3$  for BACE.

Table 3: Size generalizability evaluated by the graph classification performance on small test graphs and large test graphs. The performance is reported by the average F1 scores and its standard deviation. **+SAGPool (threshold)** means that we apply the thresholded SAG pooling [18, 20] to that model. **+SIA** means that we apply our proposed Size-Insensitive Attention to that model. Highest performance among different models is highlighted in orange.

Datasets	BBBP		BACE		PROTEINS	
Models	Small	Large	Small	Large	Small	Large
<b>MLP</b>	92.66 $\pm$ 1.72	58.39 $\pm$ 4.63	61.75 $\pm$ 4.64	21.18 $\pm$ 9.68	36.15 $\pm$ 2.28	21.55 $\pm$ 1.34
<b>MLP+SAGPool (threshold)</b>	88.3 $\pm$ 2.84	59.02 $\pm$ 17.70	61.03 $\pm$ 3.28	40.66 $\pm$ 4.81	67.78 $\pm$ 7.11	13.04 $\pm$ 5.02
<b>MLP+SIA</b>	91.07 $\pm$ 0.88	59.43 $\pm$ 3.0	64.48 $\pm$ 1.22	31.36 $\pm$ 15.19	45.02 $\pm$ 8.18	36.42 $\pm$ 13.83
<b>GCN</b>	90.66 $\pm$ 1.28	64.45 $\pm$ 3.68	64.52 $\pm$ 5.27	27.08 $\pm$ 13.66	72.35 $\pm$ 2.58	40.49 $\pm$ 3.23
<b>GCN+SAGPool (threshold)</b>	88.51 $\pm$ 2.94	66.46 $\pm$ 16.11	52.94 $\pm$ 7.99	47.87 $\pm$ 7.6	60.75 $\pm$ 3.09	5.98 $\pm$ 3.26
<b>GCN+SIA</b>	91.53 $\pm$ 1.57	71.84 $\pm$ 5.33	66.46 $\pm$ 2.63	51.96 $\pm$ 3.47	71.5 $\pm$ 1.89	37.86 $\pm$ 3.06
<b>GIN</b>	90.24 $\pm$ 1.8	67.27 $\pm$ 6.59	56.28 $\pm$ 7.35	22.97 $\pm$ 9.45	73.37 $\pm$ 1.8	45.19 $\pm$ 5.07
<b>GIN+SAGPool (threshold)</b>	89.95 $\pm$ 2.32	67.47 $\pm$ 15.2	58.52 $\pm$ 5.36	16.67 $\pm$ 11.98	65.38 $\pm$ 13.46	25.77 $\pm$ 24.54
<b>GIN+SIA</b>	90.48 $\pm$ 2.28	70.01 $\pm$ 9.97	56.72 $\pm$ 3.16	25.06 $\pm$ 5.75	72.89 $\pm$ 1.8	47.68 $\pm$ 6.04
<b>GAT</b>	92.66 $\pm$ 0.73	68.37 $\pm$ 4.87	70.14 $\pm$ 4.65	42.94 $\pm$ 4.4	72.94 $\pm$ 2.77	42.32 $\pm$ 5.93
<b>GAT+SAGPool (threshold)</b>	89.9 $\pm$ 2.15	45.74 $\pm$ 19.36	66.1 $\pm$ 6.44	38.54 $\pm$ 15.45	59.89 $\pm$ 4.53	10.6 $\pm$ 5.34
<b>GAT+SIA</b>	93.56 $\pm$ 0.74	68.76 $\pm$ 2.35	69.43 $\pm$ 5.92	44.59 $\pm$ 9.25	75.01 $\pm$ 2.95	51.19 $\pm$ 5.02
<b>FAGCN</b>	90.63 $\pm$ 2.56	60.7 $\pm$ 4.01	55.77 $\pm$ 4.72	21.0 $\pm$ 18.54	68.38 $\pm$ 3.9	46.81 $\pm$ 8.08
<b>FAGCN+SAGPool (threshold)</b>	83.08 $\pm$ 4.26	58.47 $\pm$ 17.34	58.78 $\pm$ 4.28	33.99 $\pm$ 14.97	63.41 $\pm$ 9.85	50.09 $\pm$ 16.49
<b>FAGCN+SIA</b>	92.01 $\pm$ 1.5	70.23 $\pm$ 15.87	60.84 $\pm$ 5.35	29.25 $\pm$ 11.18	68.38 $\pm$ 3.07	49.5 $\pm$ 8.42
<b>GNNML3</b>	91.52 $\pm$ 1.76	59.13 $\pm$ 8.28	61.95 $\pm$ 6.95	18.01 $\pm$ 12.23	69.66 $\pm$ 4.48	34.69 $\pm$ 5.36
<b>GNNML3+SAGPool (threshold)</b>	87.59 $\pm$ 2.9	47.5 $\pm$ 13.57	57.21 $\pm$ 6.47	35.88 $\pm$ 26.14	54.85 $\pm$ 9.96	24.79 $\pm$ 31.29
<b>GNNML3+SIA</b>	93.04 $\pm$ 0.91	65.4 $\pm$ 4.51	62.06 $\pm$ 3.48	40.06 $\pm$ 17.68	72.14 $\pm$ 2.29	52.93 $\pm$ 7.78

## 5.5 Effectiveness of Proposed Strategy

In this subsection, we examine the effectiveness of SIA.

**Baselines** We consider six neural network models. Each model consists of three layers, with a global max pooling layer employed in the final layer. The baseline models are: Multilayer Perceptron (MLP), GCN [17], GAT [27], GIN [31], FAGCN [6], and GNNML3 [2]. We also consider thresholded SAG pooling [18, 20] as a baseline strategy to be combined with the baseline models. **Upon paper acceptance, we will release the code for SIA.**

**Main Results** Table 3 displays the average and standard deviation of F1 scores assessed on small and large test sets for various models utilizing different strategies. The evaluation is conducted on the BBBP, BACE, and PROTEINS datasets. The highest performance in small and large test sets is highlighted in orange. Our observations are as follows: firstly, in comparison to the original pooling method, SIA consistently enhances performance on the large test set, with minimal exceptions, resulting in performance boosts of up to 22%. Secondly, the improved generalizability of SIA does not come at the expense of performance degradation on the small test set. In fact, SIA outperforms the baselines in more than half of the cases for small test sets and yields comparable results in the remaining cases. These findings demonstrate that SIA is model agnostic and effectively improves the size generalizability of GNNs.

## 6 Related Work

**Size-generalizable Neural Networks for Graph Data.** Size-generalizable neural networks for graph data were firstly studied in various application areas. In the field of algorithmic reasoning, [33, 28] discovered that neural networks are capable of generalizing effectively to larger graphs than the ones used during training, provided that the attention weights are properly supervised. In the field of physical simulation, [24] presented a model to simulate complex physical domains, which can generalize from single-timestep predictions with thousands of particles during training, to different initial conditions, thousands of timesteps, and at least an order of magnitude more particles at test time. Later, more works on the fundamental understanding of GNN’s size generalizability were proposed. [18] found that using attention with proper thresholding can improve the size generalizability of GNNs. [36] argued that GNNs’ performance degradation on larger graphs can be attributed to the changes in the local degree patterns. As a result, they proposed two domain adaptation strategies to improve generalizability to larger graphs. [7] simulated a size shift in the training graphs via graph coarsening, and proposed a regularization that makes the model robust to the shift. [5] used a causal model to learn approximately invariant representations that better extrapolate between train and test data. [35] studied out-of-distribution in general, and introduced an environment inference model to identify the latent factors that impact data generation from different distributions in a fully data-driven manner. Prior works have not utilized spectral analyses, and many do not specify how variations in graph size affect structural properties.

**Graph Neural Networks with Structural Attention.** Previous works have also explicitly used the structural features in their attention mechanisms for various purposes. [19, 25, 22] used structural attention to improve GNNs’ in-distribution generalization in the node/graph classification tasks. [14] incorporated structural information into the embedding learning process for heterogeneous networks, while [32] leveraged degree information to enhance GNNs’ performance on heterophilous graphs. In contrast, we use structural attention to improve the size generalizability of GNNs.

## 7 Conclusion

We investigate the size generalizability of GNNs on biological data. We observe a distribution shift in the eigenvalues of the normalized Laplacian/adjacency matrix between small and large graphs, which indicates the differences in the global node connectivity associated with the node closeness centrality. We further observe that graphs of different sizes share similar local connectivity, which can be leveraged to improve size generalizability. Based on the spectral insights and observations from real biological datasets, we propose a model-agnostic strategy, SIA, that utilizes size-irrelevant local structural features to guide learning. Our approach improves the graph classification performance of

various GNNs on small and large graphs, indicating the potential for more effective use of GNNs in real-world applications.

## References

- [1] Muhammet Balcilar, Renton Guillaume, Pierre Héroux, Benoit Gaüzère, Sébastien Adam, and Paul Honeine. Analyzing the expressive power of graph neural networks in a spectral perspective. In *Proceedings of the International Conference on Learning Representations (ICLR)*, 2021.
- [2] Muhammet Balcilar, Pierre Héroux, Benoit Gauzere, Pascal Vasseur, Sébastien Adam, and Paul Honeine. Breaking the limits of message passing graph neural networks. In *International Conference on Machine Learning*, pages 599–608. PMLR, 2021.
- [3] Alex Bavelas. A mathematical model for group structures. *Human organization*, 7(3):16–30, 1948.
- [4] Michele Berlingerio, Danai Koutra, Tina Eliassi-Rad, and Christos Faloutsos. A scalable approach to size-independent network similarity. *ArXiv Preprint ArXiv: 12092684*, 2012.
- [5] Beatrice Bevilacqua, Yangze Zhou, and Bruno Ribeiro. Size-invariant graph representations for graph classification extrapolations. In *International Conference on Machine Learning*, pages 837–851. PMLR, 2021.
- [6] Deyu Bo, Xiao Wang, Chuan Shi, and Huawei Shen. Beyond low-frequency information in graph convolutional networks. *arXiv preprint arXiv:2101.00797*, 2021.
- [7] Davide Buffelli, Pietro Lio, and Fabio Vandin. Sizeshiftreg: a regularization method for improving size-generalization in graph neural networks. In *Advances in Neural Information Processing Systems*, 2022.
- [8] Jeff Cheeger. A lower bound for the smallest eigenvalue of the laplacian. In *Problems in analysis*, pages 195–200. Princeton University Press, 2015.
- [9] Fan RK Chung. *Spectral graph theory*, volume 92. American Mathematical Soc., 1997.
- [10] Gabriele Corso, Luca Cavalleri, Dominique Beaini, Pietro Liò, and Petar Veličković. Principal neighbourhood aggregation for graph nets. *Advances in Neural Information Processing Systems*, 33:13260–13271, 2020.
- [11] Michaël Defferrard, Xavier Bresson, and Pierre Vandergheynst. Convolutional neural networks on graphs with fast localized spectral filtering. In *NeurIPS*, 2016.
- [12] Justin Gilmer, Samuel S Schoenholz, Patrick F Riley, Oriol Vinyals, and George E Dahl. Neural message passing for quantum chemistry. In *International conference on machine learning*, pages 1263–1272. PMLR, 2017.
- [13] Will Hamilton, Zhitaoy Ying, and Jure Leskovec. Inductive representation learning on large graphs. In *NeurIPS*, 2017.
- [14] Huiting Hong, Hantao Guo, Yucheng Lin, Xiaoqing Yang, Zang Li, and Jieping Ye. An attention-based graph neural network for heterogeneous structural learning. In *Proceedings of the AAAI conference on artificial intelligence*, volume 34, pages 4132–4139, 2020.
- [15] W Hu, B Liu, J Gomes, M Zitnik, P Liang, V Pande, and J Leskovec. Strategies for pre-training graph neural networks. In *International Conference on Learning Representations (ICLR)*, 2020.
- [16] Weihua Hu, Matthias Fey, Marinka Zitnik, Yuxiao Dong, Hongyu Ren, Bowen Liu, Michele Catasta, and Jure Leskovec. Open graph benchmark: Datasets for machine learning on graphs. *Advances in neural information processing systems*, 33:22118–22133, 2020.
- [17] Thomas N. Kipf and Max Welling. Semi-supervised classification with graph convolutional networks. In *International Conference on Learning Representations (ICLR)*, 2017.
- [18] Boris Knyazev, Graham W Taylor, and Mohamed Amer. Understanding attention and generalization in graph neural networks. *Advances in neural information processing systems*, 32, 2019.
- [19] John Boaz Lee, Ryan Rossi, and Xiangnan Kong. Graph classification using structural attention. In *Proceedings of the 24th ACM SIGKDD International Conference on Knowledge Discovery & Data Mining*, pages 1666–1674, 2018.

- [20] Junhyun Lee, Inyeop Lee, and Jaewoo Kang. Self-attention graph pooling. In *International conference on machine learning*, pages 3734–3743. PMLR, 2019.
- [21] Ron Levie, Federico Monti, Xavier Bresson, and Michael M Bronstein. Cayleynets: Graph convolutional neural networks with complex rational spectral filters. *IEEE Transactions on Signal Processing*, 67(1):97–109, 2018.
- [22] Xuanjie Lin, Hantong Jiang, Liquan Wang, Yongsheng Ren, Wenhui Ma, and Shu Zhan. 3d-structure-attention graph neural network for crystals and materials. *Molecular Physics*, 120(11):e2077258, 2022.
- [23] Christopher Morris, Nils M. Kriege, Franka Bause, Kristian Kersting, Petra Mutzel, and Marion Neumann. Tudataset: A collection of benchmark datasets for learning with graphs. In *ICML 2020 Workshop on Graph Representation Learning and Beyond (GRL+ 2020)*, 2020.
- [24] Alvaro Sanchez-Gonzalez, Jonathan Godwin, Tobias Pfaff, Rex Ying, Jure Leskovec, and Peter Battaglia. Learning to simulate complex physics with graph networks. In *International conference on machine learning*, pages 8459–8468. PMLR, 2020.
- [25] Aravind Sankar, Yanhong Wu, Liang Gou, Wei Zhang, and Hao Yang. Dysat: Deep neural representation learning on dynamic graphs via self-attention networks. In *Proceedings of the 13th international conference on web search and data mining*, pages 519–527, 2020.
- [26] Wasserman Stanley, Faust Katherine, et al. Social network analysis: Methods and applications. *Cambridge: Cambridge University*, 1994.
- [27] Petar Veličković, Guillem Cucurull, Arantxa Casanova, Adriana Romero, Pietro Liò, and Yoshua Bengio. Graph Attention Networks. *International Conference on Learning Representations (ICLR)*, 2018.
- [28] Petar Veličković, Rex Ying, Matilde Padovano, Raia Hadsell, and Charles Blundell. Neural execution of graph algorithms. In *International Conference on Learning Representations*, 2020.
- [29] Cédric Villani et al. *Optimal transport: old and new*, volume 338. Springer, 2009.
- [30] Zhenqin Wu, Bharath Ramsundar, Evan N Feinberg, Joseph Gomes, Caleb Geniesse, Aneesh S Pappu, Karl Leswing, and Vijay Pande. Moleculenet: a benchmark for molecular machine learning. *Chemical science*, 9(2):513–530, 2018.
- [31] Keyulu Xu, Weihua Hu, Jure Leskovec, and Stefanie Jegelka. How powerful are graph neural networks? *International Conference on Learning Representations*, 2018.
- [32] Yujun Yan, Milad Hashemi, Kevin Swersky, Yaoqing Yang, and Danai Koutra. Two sides of the same coin: Heterophily and oversmoothing in graph convolutional neural networks. In *2022 IEEE International Conference on Data Mining (ICDM)*, pages 1287–1292. IEEE, 2022.
- [33] Yujun Yan, Kevin Swersky, Danai Koutra, Parthasarathy Ranganathan, and Milad Hashemi. Neural execution engines: Learning to execute subroutines. *Advances in Neural Information Processing Systems*, 33:17298–17308, 2020.
- [34] Yujun Yan, Jiong Zhu, Marlena Duda, Eric Solarz, Chandra Sripada, and Danai Koutra. Groupinn: Grouping-based interpretable neural network for classification of limited, noisy brain data. In *proceedings of the 25th ACM SIGKDD international conference on knowledge discovery & data mining*, pages 772–782, 2019.
- [35] Nianzu Yang, Kaipeng Zeng, Qitian Wu, Xiaosong Jia, and Junchi Yan. Learning substructure invariance for out-of-distribution molecular representations. In *Advances in Neural Information Processing Systems*, 2022.
- [36] Gilad Yehudai, Ethan Fetaya, Eli Meir, Gal Chechik, and Haggai Maron. From local structures to size generalization in graph neural networks. In *International Conference on Machine Learning*, pages 11975–11986. PMLR, 2021.
- [37] Zhitao Ying, Jiaxuan You, Christopher Morris, Xiang Ren, Will Hamilton, and Jure Leskovec. Hierarchical graph representation learning with differentiable pooling. In *NeurIPS*, pages 4800–4810, 2018.
- [38] Muhan Zhang, Zhicheng Cui, Marion Neumann, and Yixin Chen. An end-to-end deep learning architecture for graph classification. In *Proceedings of the AAAI conference on artificial intelligence*, volume 32, 2018.

## A Dataset

In this section, we provide additional details about the datasets utilized in our study. We utilize three pre-processed biological datasets, namely BBBP and BACE from the Open Graph Benchmark [16], and PROTEINS from TuDataset [23], for graph classification in our experiments. Each graph in BBBP and BACE represents a molecule, where nodes are atoms, and edges are chemical bonds. Each node has a 9-dimensional feature vector, which contains its atomic number and chirality, as well as other additional atom features such as formal charge and whether the atom is in the ring or not [16]. In the PROTEINS dataset, nodes correspond to amino acids, and an edge connects two nodes if their distance is less than 6 Angstroms. Each node is associated with a 3-dimensional feature vector representing the type of secondary structure elements, such as helix, sheet, or turn. The description of each dataset is summarized as follows:

- **BBBP**: The blood-brain barrier penetration (BBBP) dataset comes from a study on the modeling and the prediction of barrier permeability. It includes binary labels of over 2000 compounds on their permeability properties [30].
- **BACE**: The BACE dataset provides quantitative (IC50) and qualitative (binary label) binding results for a set of inhibitors of human  $\beta$ -secretase 1 (BACE-1). It contains 1522 compounds with their 2D structures and binary labels [30].
- **PROTEINS**: The PROTEINS dataset comprises the macromolecule graphs of proteins and binary labels of the protein function (being an enzyme or not) for a total of 1113 samples [23].

Table 4: Label Distributions of BBBP, BACE, and PROTEINS for the entire dataset, the smallest 50% subset, and the largest 10% subset.

Dataset		BBBP	BACE	PROTEINS
Entire Dataset	Number of Class 0 Samples	479	822	663
	Number of Class 1 Samples	1560	691	450
Smallest 50%	Number of Class 0 Samples	138	501	232
	Number of Class 1 Samples	882	256	325
Largest 10%	Number of Class 0 Samples	122	53	101
	Number of Class 1 Samples	82	99	11

## B Label Imbalance and Distribution Shifts

In this section, we discuss the techniques employed to address the challenges of class imbalance and label distribution shifts between small and large graphs.

Table 4 presents the respective class sizes in each dataset in terms of the total size, smallest 50% size, and the largest 10% size. This Table reveals two main issues. Firstly, none of the datasets demonstrate balanced label distributions, with BBBP displaying a particularly pronounced class imbalance. Secondly, both the small 50% and the largest 10% graphs exhibit class imbalance, and there is a notable difference in the label distribution between these subsets. To mitigate these issues, we carefully split our data and apply the upsampling technique.

**Data splits.** For each dataset, we create four distinct splits: train, validation, small\_test, and large\_test. The large\_test split consists of graphs with significantly larger sizes compared to the other splits. To generate the train, validation, and small\_test subsets, we initially select the smallest 50% of graphs from the dataset. The division among these subsets follows a ratio of 0.7:0.15:0.15, respectively. Importantly, we ensure that the data is split for each class using the same ratio, thereby maintaining

consistent label distributions across the train, validation, and small\_test subsets. Next, we generate the large\_test subset by selecting the same number of graphs per class as in the small\_test subset. The selection process begins with the largest graph within each class and ensures that the large\_test subset maintains the same class distribution as the small\_test subset. Table 5 shows the class size obtained after applying this operation.

**Upsampling.** As can be seen in Table 4, even after performing the appropriate data split, each dataset still exhibits varying degrees of class imbalance. To avoid training an extremely biased model, we adopt the upsampling technique during the training process. Specifically, we upsample the graphs in class 0 of BBBP at a ratio of 6, the graphs in class 1 of BACE at a ratio of 2, and  $\frac{2}{3}$  of the graphs in class 0 of PROTEINS at a ratio of 2. By doing so, a GNN model trained on the current training split can have a decent performance on the small\_test samples. For a fair measurement, we use **F1** as the evaluation metric throughout this paper.

Table 5: Label distributions after proper data splits. both the Both the small\_test and large\_test subsets now have the same class distribution.

	Dataset	BBBP	BACE	PROTEINS
Train	Number of Class 0 Samples	96	350	140
	Number of Class 1 Samples	617	179	210
Val	Number of Class 0 Samples	22	76	30
	Number of Class 1 Samples	133	39	46
Small_test	Number of Class 0 Samples	20	75	30
	Number of Class 1 Samples	132	38	45
Large_test	Number of Class 0 Samples	20	75	30
	Number of Class 1 Samples	132	38	45

## C Training Details

In this section, we provide the details of our training process for the purpose of reproducibility.

To ensure fair comparisons, we maintain consistent hyperparameter settings across all experiments. Specifically, we use a batch size of 30 and a learning rate of 0.001. The Adam optimizer is employed without gradient clipping. For the baseline models, we utilize 3 graph convolution layers with a global max pooling. The previously described upsampling technique is applied to all methods. To prevent overfitting, we implement early stopping using the validation loss as the criterion, with a patience period of 50 epochs. Each method is executed 5 times, and we report the average result along with the standard deviation in Table 3.

To ensure consistency with the original papers, we set the other hyperparameters of each baseline model to match the values specified in their respective papers (except for the threshold in SAG pooling). In the case of thresholded SAG pooling, we conduct tuning with thresholds from the set 0.1, 0.2, 0.05, 0.5. Based on the validation results, we determine the threshold values of 0.1 for BBBP, 0.05 for BACE, and 0.5 for PROTEINS. Regarding SIA, it only involves one hyperparameter, namely  $h$ -hop closeness. We choose  $h = 3$  for BBBP and BACE, and  $h = 2$  for PROTEINS. The rationale for these specific choices is further explained in Section 5.4 and Appendix E.

## D Scaled Eigenvectors

In this section, we study whether the distributions of scaled eigenvectors (Section 3) change with graph size. Figure 4 shows the distance of the graphs, measured by the Wasserstein distance

Table 6: Average Wasserstein distance between graphs of similar size and graphs of different sizes based on **Scaled Eigenvectors**. The relative difference is computed by the difference of the average Wasserstein distance normalized by the average Wasserstein distance of similar graphs.

Datasets	Different sizes	Similar sizes	Relative Difference
BBBP	0.015	0.022	42.9%
BACE	0.012	0.017	40.6%
PROTEINS	0.016	0.025	50.7%

between the distributions of scaled eigenvectors ( $\sqrt{n} \cdot \mathbf{U}_1$ ).  $\mathbf{U}_1$  represents the normalized eigenvector corresponding to the largest eigenvalue. Though both  $\mathbf{U}_1$  and  $-\mathbf{U}_1$  are normalized eigenvectors for the same eigenvalue, we obtain  $\mathbf{U}_1$  such that its first entry is non-negative. Though we only show the analysis for eigenvector  $\mathbf{U}_1$ , the other eigenvectors exhibit similar patterns. In Figure 4, dark blue represents high similarity while light red represents low similarity. As can be seen in Figure 4, there is a narrow dark blue band along the diagonal in the three subplots. This indicates that graphs with very comparable sizes have similar scaled eigenvector distributions, but the correlation, in this case, is weaker than that in the case of eigenvalues. To verify it quantitatively, we compute the graph distance of similar graphs and different graphs in Table 6. Graphs of similar size include 20 graphs whose size is closest to the graph of interest, and graphs of different sizes are the remaining graphs. From the table, we can see that the Wasserstein distance between the graphs of different sizes is noticeably larger than the distance between graphs of similar size. Based on the conclusion in Section 3, the weak correlation between the scaled eigenvectors and graph size also hurts GNNs’ ability to generalize to larger graphs.

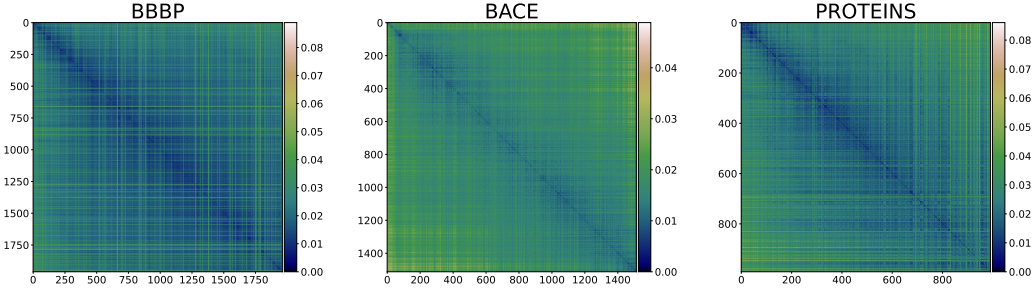


Figure 4: Graph distance based on the distributions of scaled eigenvectors ( $\sqrt{n} \cdot \mathbf{U}_1$ ). Graphs are sorted from small to large, and the pixel  $(i,j)$  represents the distance between the  $i$ -th and  $j$ -th graphs. Dark blue represents a small distance (high similarity) while light red represents a large distance (low similarity). **The distributions show a weak correlation with the graph size.**

## E Local Closeness

In this section, we provide justifications for the selection of the neighborhood size  $h$ , which is used to calculate the local closeness. We present analogous plots to those shown in Section 5.4 for the BBBP and PROTEINS datasets. Figure 5 and Figure 6 show the distances for the sorted graphs, which are measured by the Wasserstein distance between the empirical distributions of  $h$ -hop local closeness for the BBBP and the PROTEINS dataset. Analyzing the BBBP dataset, we observe that both small and large graphs display similar distributions of local closeness within their two- or three-hop neighborhoods, as evidenced by the absence of a distinct blue band along the diagonal in the corresponding plots. However, the four-hop local closeness varies with the graph size, as indicated by the presence of a noticeable wide blue band along the diagonal in the four-hop plot. In the case of the PROTEINS dataset, we observe that only the two-hop local closeness does not exhibit a clear dependence on the graph size. Taking these findings into consideration, we determine that a neighborhood size of  $h = 3$  is suitable for the BBBP dataset, while a neighborhood size of  $h = 2$  is appropriate for the PROTEINS dataset.

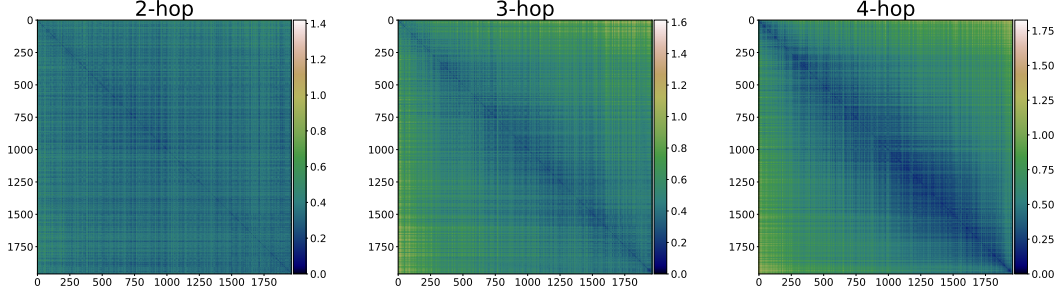


Figure 5: Graph distance based on  $h$ -hop local closeness for BBBP (left to right:  $h=2$ ,  $h=3$ , and  $h=4$ ). Graphs are sorted from small to large and we follow the same procedures as Figure 2. The dependence of small-hop (two-hop and three-hop) local closeness on graph size is not evident.

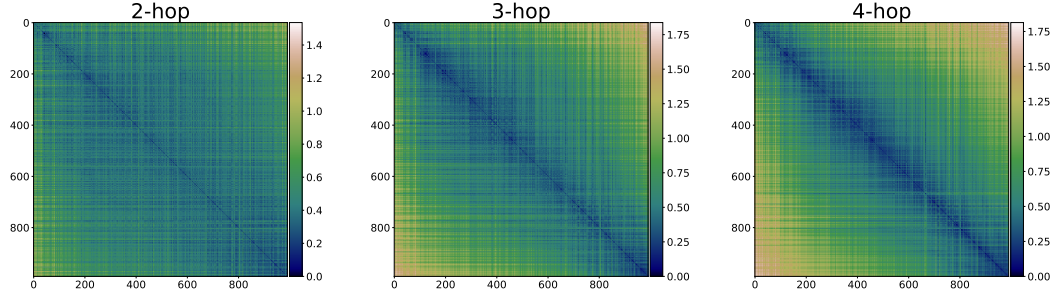


Figure 6: Graph distance based on  $h$ -hop local closeness for PROTEINS (left to right:  $h=2$ ,  $h=3$ , and  $h=4$ ). Graphs are sorted from small to large and we follow the same procedures as Figure 2. The dependence of two-hop local closeness on graph size is not evident.

## F Ablation Studies

In this section, we conducted a thorough ablation study on our selection of input structural features as discussed in Section 4. Recall that we use the following structural features for node  $v_i$  in SIA:

$$\mathbf{c}_i = [C^h(v_i), \max(\{C^h(v_j)\}), \min(\{C^h(v_j)\}), \text{avg}(\{C^h(v_j)\}), \text{std}(\{C^h(v_j)\})]^\top, v_j \in \mathcal{N}_i^1 \quad (6)$$

We further explore two alternative constructions of  $\mathbf{c}_i$ . First, we consider the scenario where  $\mathbf{c}_i$  is a scalar value representing the  $h$ -hop local closeness of node  $v_i$ :

$$\mathbf{c}_i = [C^h(v_i)] \quad (7)$$

Second, instead of computing maximum, minimum, average, and standard deviation of the  $h$ -hop closeness for the nodes in  $v_i$ 's immediate neighborhood  $\mathcal{N}_i^1$ , we compute these statistic measures for the nodes in the  $h$ -hop neighborhood of  $v_i$ .

$$\mathbf{c}_i = [C^h(v_i), \max(\{C^h(v_j)\}), \min(\{C^h(v_j)\}), \text{avg}(\{C^h(v_j)\}), \text{std}(\{C^h(v_j)\})]^\top, v_j \in \mathcal{N}_i^h \quad (8)$$

We use the following abbreviations to represent different variants:  $h$ -hop local closeness only (Equation (7)): LC; local closeness plus the additional features taken from the entire  $h$ -hop neighborhood (Equation (8)): LC+EntireHop; local closeness plus the additional features taken from the *one-hop* neighborhood (Equation (6)), which is our proposed method SIA: LC+OneHop(SIA). We adhere to the same experimental settings, run each variant on the three datasets, and present the respective results in Table 7. For comparison purposes, we also include the original results without applying any structural attention in the first row. We highlight in orange the best performance among the three variants per dataset for both small and large test graphs.

Table 7: Size generalizability evaluated by the graph classification performance on small and large test graphs. The performance is reported as the average F1 scores and its standard deviation. The first row in each category represents the original performance without applying any structural attention. +LC means attention with local closeness only; +LC+EntireHop means attention with local closeness plus the additional features taken from the entire  $h$ -hop neighborhood; +LC+OneHop means attention with local closeness plus the additional features taken from the one-hop neighborhood, which is our proposed method SIA. Best performance among the three variants in small and large test sets is highlighted in orange.

Datasets	BBBP		Bace		PROTEINS	
Models	Small	Large	Small	Large	Small	Large
MLP	92.66 $\pm$ 1.72	58.39 $\pm$ 4.63	61.75 $\pm$ 4.64	21.18 $\pm$ 9.68	36.15 $\pm$ 2.28	21.55 $\pm$ 1.34
MLP+LC	90.86 $\pm$ 1.65	56.75 $\pm$ 5.37	61.66 $\pm$ 3.19	30.07 $\pm$ 4.88	43.32 $\pm$ 8.02	29.44 $\pm$ 8.97
MLP+LC+EntireHop	90.58 $\pm$ 0.55	58.99 $\pm$ 7.75	62.26 $\pm$ 2.09	22.53 $\pm$ 4.02	55.24 $\pm$ 9.2	38.04 $\pm$ 19.01
MLP+LC+OneHop(SIA)	91.07 $\pm$ 0.88	59.43 $\pm$ 3.0	64.48 $\pm$ 1.22	31.36 $\pm$ 15.19	45.02 $\pm$ 8.18	36.42 $\pm$ 13.83
GCN	90.66 $\pm$ 1.28	64.45 $\pm$ 3.68	64.52 $\pm$ 5.27	27.08 $\pm$ 13.66	72.35 $\pm$ 2.58	40.49 $\pm$ 3.23
GCN+LC	91.20 $\pm$ 0.88	66.54 $\pm$ 8.02	65.23 $\pm$ 2.55	35.68 $\pm$ 14.58	72.81 $\pm$ 3.28	42.22 $\pm$ 5.17
GCN+LC+EntireHop	91.03 $\pm$ 1.49	63.52 $\pm$ 8.65	65.33 $\pm$ 5.12	35.50 $\pm$ 9.57	70.30 $\pm$ 3.77	38.32 $\pm$ 4.88
GCN+LC+OneHop(SIA)	91.53 $\pm$ 1.57	71.84 $\pm$ 5.33	66.46 $\pm$ 2.63	51.96 $\pm$ 3.47	71.5 $\pm$ 1.89	37.86 $\pm$ 3.06
GIN	90.24 $\pm$ 1.8	67.27 $\pm$ 6.59	56.28 $\pm$ 7.35	22.97 $\pm$ 9.45	73.37 $\pm$ 1.8	45.19 $\pm$ 5.07
GIN+LC	91.92 $\pm$ 0.61	74.42 $\pm$ 7.81	57.04 $\pm$ 4.09	20.92 $\pm$ 3.36	74.89 $\pm$ 3.65	48.79 $\pm$ 3.13
GIN+LC+EntireHop	90.64 $\pm$ 1.52	69.55 $\pm$ 10.77	58.75 $\pm$ 4.52	26.67 $\pm$ 8.57	71.66 $\pm$ 2.85	44.50 $\pm$ 7.64
GIN+LC+OneHop(SIA)	90.48 $\pm$ 2.28	70.01 $\pm$ 9.97	56.72 $\pm$ 3.16	25.06 $\pm$ 5.75	72.89 $\pm$ 1.8	47.68 $\pm$ 6.04
GAT	92.66 $\pm$ 0.73	68.37 $\pm$ 4.87	70.14 $\pm$ 4.65	42.94 $\pm$ 4.4	72.94 $\pm$ 2.77	42.32 $\pm$ 5.93
GAT+LC	92.25 $\pm$ 0.42	68.6 $\pm$ 2.46	67.37 $\pm$ 2.75	35.84 $\pm$ 14.94	75.18 $\pm$ 2.54	44.91 $\pm$ 4.37
GAT+LC+EntireHop	92.13 $\pm$ 0.68	71.44 $\pm$ 5.21	67.69 $\pm$ 3.88	34.71 $\pm$ 18.25	73.59 $\pm$ 2.72	45.24 $\pm$ 6.63
GAT+LC+OneHop(SIA)	93.56 $\pm$ 0.74	68.76 $\pm$ 2.35	69.43 $\pm$ 5.92	44.59 $\pm$ 9.25	75.01 $\pm$ 2.95	51.19 $\pm$ 5.02
FAGCN	90.63 $\pm$ 2.56	60.7 $\pm$ 4.01	55.77 $\pm$ 4.72	21.0 $\pm$ 18.54	68.38 $\pm$ 3.9	46.81 $\pm$ 8.08
FAGCN+LC	90.71 $\pm$ 1.72	65.88 $\pm$ 5.58	59.17 $\pm$ 7.13	18.66 $\pm$ 15.05	66.72 $\pm$ 4.52	38.2 $\pm$ 6.79
FAGCN+LC+EntireHop	91.13 $\pm$ 1.83	69.85 $\pm$ 14.8	57.04 $\pm$ 8.28	22.5 $\pm$ 13.98	68.49 $\pm$ 4.26	48.8 $\pm$ 7.7
FAGCN+LC+OneHop(SIA)	92.01 $\pm$ 1.5	70.23 $\pm$ 15.87	60.84 $\pm$ 5.35	29.25 $\pm$ 11.18	68.39 $\pm$ 3.07	49.5 $\pm$ 8.42
GNNML3	91.52 $\pm$ 1.76	59.13 $\pm$ 8.28	61.95 $\pm$ 6.95	18.01 $\pm$ 12.23	69.66 $\pm$ 4.48	34.69 $\pm$ 5.36
GNNML3+LC	92.26 $\pm$ 0.44	62.37 $\pm$ 5.49	63.83 $\pm$ 3.21	21.99 $\pm$ 19.57	69.99 $\pm$ 3.49	41.01 $\pm$ 10.44
GNNML3+LC+EntireHop	93.33 $\pm$ 1.41	67.45 $\pm$ 8.9	62.34 $\pm$ 3.65	42.19 $\pm$ 4.18	71.31 $\pm$ 2.51	43.66 $\pm$ 12.74
GNNML3+LC+OneHop(SIA)	93.04 $\pm$ 0.91	65.4 $\pm$ 4.51	62.06 $\pm$ 3.48	40.06 $\pm$ 17.68	72.14 $\pm$ 2.29	52.93 $\pm$ 7.78

Table 8: Performance summary of LC, LC+EntireHop, and LC+OneHop. Arrows indicate whether higher counts ( $\uparrow$ ) or lower counts ( $\downarrow$ ) are desirable. The best variant for each criterion is highlighted in orange.

	LC	LC+EntireHop	LC+OneHop
# achieve the best performance ( $\uparrow$ )	10	9	19
# perform better on large test sets compared with the original method ( $\uparrow$ )	13	14	17
# perform worse on small test sets compared with the original method ( $\downarrow$ )	4	5	4

To gain a better understanding of the results presented in Table 7 and make informed decisions regarding the optimal features, we provide a summary of the performance for different variants in Table 8. This summary focuses on several key aspects. Firstly, we track the frequency at which a variant achieves the best performance, either on small or large test sets. Next, we examine how often a variant outperforms the original method on large test sets, which reflects the model’s ability to generalize to larger-sized inputs. Then we count how often a variant underperforms the original method on small test sets, as this indicates the extent to which we sacrifice the model’s in-distribution generalizability. Ideally, a desirable variant would frequently outperform the original method on large test sets while rarely underperforming the original method on small test sets. Based on the observations from Table 8, we can draw the following conclusions. Firstly, in 13 out of 18 cases, local closeness alone contributes to performance improvements in large test sets. These improvements can

reach up to nine percent, highlighting the effectiveness of this feature. Secondly, using the entire hop features does not necessarily lead to better overall performance compared to using local closeness alone. This may be due to the significant overlap of the  $h$ -hop neighborhoods for different nodes. Lastly, our proposed method, SIA, which incorporates both local closeness and one-hop features, achieves the best performance most frequently. It outperforms the original method in 17 out of 18 cases in the large test set, with only minor degradation in 4 cases in the small test set. These results provide strong evidence supporting the rationale behind SIA’s choice of Equation 4 as the main source of attention.